Chapter 1

Brain Tumor Segmentation from Multi-modality MRI Scans Using Machine Learning

By

Khalid Usman

MSCS-2

Supervised by

Dr. Kashif Mahmood Rajpoot

Assistant Professor

NUST-SEECS

This thesis is submitted in partial fulfilment of the requirements for the degree of Masters of Science in Computer Science (MSCS)

School of Electrical Engineering and Computer Science,
National University of Sciences and Technology (NUST),
Islamabad, Pakistan.

Chapter 1

Abstract

Brain tumor can grow anywhere in the brain, but it is commonly grown in the cells that make the brain tissues and the nerves covering the brain's outer boundary called meninges. There are two main types of brain tumor known as benign and malignant. Both these types are characterized by different symptoms and properties, e.g. benign tumor is slow growing as compared to malignant whereas malignant tumor spreads into the surrounding tissues as opposite to the benign tumor. The aim of this work is to develop a technique to detect and diagnose the tumor.

This research proposed a brain tumor segmentation method by exploring multi-modality MRI scans, since brain tumor has unpredictable shape and appearance, which is hard to be captured by a single modality. The multi-modality images are normally the scans taken by various imaging modalities e.g. MRI, PET and CT. In our case, we used the images obtained from T1, T2, T1-Contrast and FLAIR modalities of MRI acquisition. The data from MICCAI BraTS 2013 challenge is utilized, which is co-registered and skull-stripped. Histogram matching and bounding box is applied to the images of all modalities. Subsequently, the intensity, intensity differences, local neighbourhood and wavelet features are extracted to develop a system for identifying the tumor severity.

We further developed an automatic method for segmentation of brain tumor by exploring machine learning approaches, including random forest, k-nearest neighbour and ensemble algorithms of adaBoostM2 and rusBoost. We classified voxels into five classes; background, necrosis, edema, enhancing tumor and non-enhancing tumor and hierarchically computed three regions (whole tumor, core tumor and enhancing tumor) from above classes.

We applied the above mentioned machine learning approaches and found that random forest classifier is best among all classifiers tested on our dataset and the extracted features. With leave-one-out cross validation, it achieved 88% Dice overlap for whole tumor region, 75% for core tumor and 95% for enhancing tumor, which is better than the Dice overlap reported from MICCAI BraTS 2013 challenge.

Chapter 1 : Background and Introduction

1 Background and Introduction

Brain is the control center of the body, which controls every human activity. Brain has millions of nerves cells in it, which communicate to the body by sending electrical/chemical signals. There is other type of cells called the glial cells, which support neurons but may grow into brain tumor. Brain tumor can grow anywhere in the brain, but it is mostly grown by the cells that make brain tissues and nerves covering the brain's outer boundary. There are two main types of brain tumor i.e. primary and metastatic. Both these types are characterized by different symptoms and properties e.g. primary tumor arises in brain and central nervous system and usually does not spread out of brain, whereas metastatic brain tumor arises in other part of the body and spreads to brain [1].

According to a recent survey in USA, 25 out of every 100,000 adults suffer from brain tumor and two-third of them have benign brain tumor while remaining have malignant tumor [2]. National Cancer Institute estimated over 23,000 people in USA would be diagnosed with malignant brain tumor during 2014 [3]. Brain tumor is difficult to cure, because the brain has a very complex structure and tissues are interconnected with each other in a complicated manner. Extracting tumor from brain is more likely to damage the neighbouring tissues. The survival chance of patient depends on the location, type and size of tumor, patient medical history and presence or absence of metastasis. Therefore it is crucial to diagnose the tumor early so that the treatment can be initiated.

1.1 Brain Imaging

Brain tumor images can be acquired by MRI, CT and PET [4] as shown in Figure 1.

- **Magnetic Resonance Imaging (MRI)**

  MRI is known best for the imaging of soft tissues. It uses radio waves and magnetic field for imaging, therefore it is free from harmful radiation effects. MRI provides good contrast, but it is expensive and is taken by putting patient in an enclosed space.

- **Computed Tomography (CT)**

  CT is typically used for examining bone injuries, bleeding in the brain and lungs [5]. It is less expensive, but provides poor contrast. A dye agent is injected in human body to enhance the contrast of images, but dye agent can have harmful effects on kidney [6].

- **Positron Emission Tomography (PET)**

  PET shows the functional behaviour of the brain rather than the structural unlike MRI and CT. A radioactive contrast dye agent is injected into the patient's blood vessels and patient is asked to position himself on bed. Radioactive waves emit from patient's brain after some time, which are captured by sensors.

1.2 MRI Acquisition

A heavy machine as in Figure 2 with magnetic field in the range of 0.2T to 7T (typically 1.5T) is used and radio frequency signals emitted by excited hydrogen atoms in the body (present in water molecules) are detected. Images of different modality can be achieved by varying the strength of magnetic field. Images are taken in the loud sound and enclosed space of MRI scanner, where patients may feel claustrophobic. Magnetic coils are switched on and off rapidly to note the time taken by hydrogen items for realignment into equilibrium state, and image is

captured at different stages during the state change of hydrogen items. This complete process can take 15 to 45 minutes.

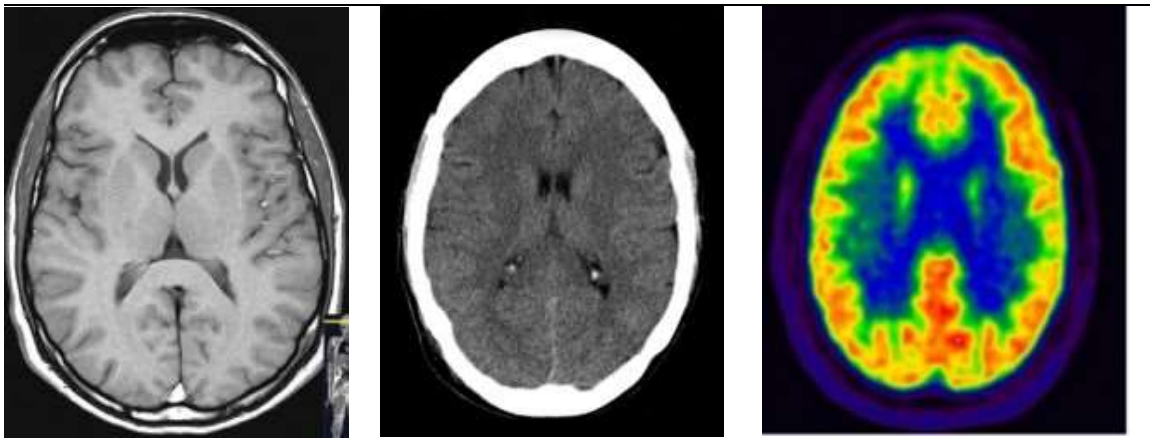

Figure 1: Imaging of brain tumor: (a) MRI, (b) CT, (c) PET [7]

Figure 2: MRI Scanning, where magnetic field is applied to capture images of brain [8].

1.2.1 Multi-modality MRI Sequences

MRI provides us the ability to obtain multiple images by varying the echo time and repetition time. Echo time interval in which signals are measured after the radio frequency excitations, while repeat time is the time interval between two successive echo times.

- **T1**

  It has short TE and TR but fast image acquisition. It provides good contrast for healthy tissues (gray matter, white matter and cerebrospinal fluid).

- **T2**

  It has long TE and TR but slow image acquisition. It provides good contrast for the tumor surrounding tissues (edema).

- **T1C**

  It is same as T1, but a contrast agent is applied to enhance the contrast.

- **FLAIR**

  It is used to nullify the signal from the fluid, suppress the effect of Cerebrospinal Fluid (CSF) and bring out the periventricular hyper intense lesion.

It is hard to fully segment and classify brain tumor from uni-modality scans, because of its complicated structure and shape. MRI provides us the ability to capture multiple images. Multi-modality images are believed to provide the detailed structure of brain which can help to efficiently classify and segment the brain tumor [1]. Figure **3** shows different MRI modalities of brain.

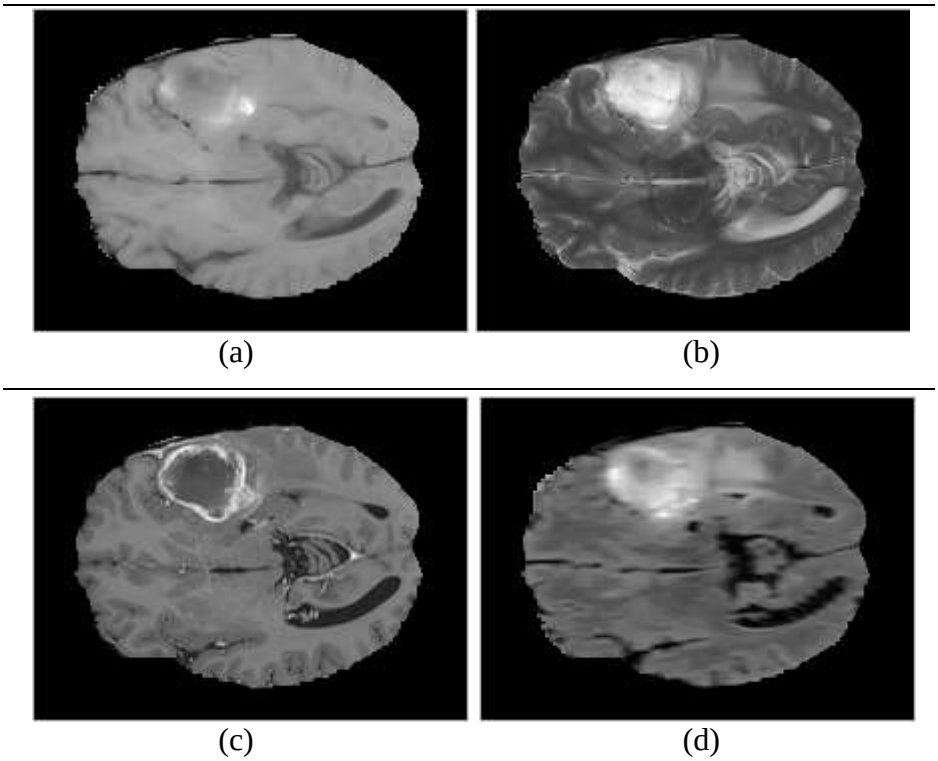

Figure 3: Brain multi-modality MRI; (a) T1, (b) T2, (c) T1C, (d) FLAIR.

1.3 Thesis Motivation

Brain tumor segmentation based on MRI images has received significant interest over last decade. Brain tumor segmentation using uni-modality MRI has been explored in many studies [9-13]. Recently, researchers have explored multi-modality MRI to increase the accuracy of tumor segmentation and classification. Machine learning and edge/region based approaches have been used with multi-modal (T1, T2, T1C and FLAIR) MRI. Classifiers like support vector machine (SVM), random forest (RF), k-nearest neighbours (kNN) are the examples of machine learning approaches whereas edge/region based approaches include deformable methods like ACM.

Segmentation algorithms can be categorized as edge/region based techniques which use active contour model (ACM) and classification/clustering techniques that rely on voxel intensities and

other features. Individual voxel is classified on the basis of feature vector [14]. Intensity, neighbourhood and other texture features are already explored on benchmark dataset [15], but to the best of our knowledge wavelet based features have not yet been explored on multi-modality MRI brain tumour data. In this work, we study the use of wavelet texture features along with various machine learning algorithms.

In the past, there was no benchmark dataset and researchers used different dataset and different modalities for segmentation. This created difficulty in comparing various algorithms' performance. MICCAI BraTS was introduced as a competition in 2012, where organizers shared multimodality brain tumor data with researchers, who were invited to develop an algorithm and perform testing on the provided data. In this way all researchers can use the same dataset, so results can be compared directly and algorithms can be ranked on the basis of performance [14].

1.4 Thesis Contributions

In this work, we used multi-modality images to fully segment and classify the brain tumor. This work makes following contributions:

i. Extracting wavelet based texture features to describe the tumor classes
ii. Exploring classifiers (KNN, RF, AdaBoostM2 and RusBoost) for brain tumor segmentation

1.5 Thesis Organization

This thesis is structured as following.

Chapter 2 presents the previous work on brain tumor segmentation and classification. Chapter 3 introduces the proposed methodology leading to results in Chapter 4. Chapter 5 provides conclusion and future work directions.

Chapter 2 : Literature Review

2 Literature Review

Segmentation is a challenging process because tumor exhibits inhomogeneous intensities and unclear boundaries. Intensity normalization or bias field correction is often applied to balance the effect of magnetic field inhomogeneity [1]. Previously MRI does not produce satisfactory results for brain tumor segmentation and classification due to low frequency signals and biasness of magnetic field, so the issue is resolved by using bias field correction. Intensities, neighbourhood and texture analysis are common features used by researchers. Various machine learning and edge/region based techniques used in segmentation are summarized in Table **1**.

In Table 1 we present a concise review of the previous work, where different segmentation algorithms based on either machine learning or edge/region based technique are used. Few techniques are fully automatic, while remaining need user involvement. Researchers used different performance measures; most of them used Dice similarity co-efficient, while remaining used Jaccard, similarity index, tanimoto or true positive.

Rexilius *et al.* [10] proposed a new region growing method for segmentation of brain tumor. Probabilistic model is used to achieve the initial segmentation, which is further refined by region growing to give better segmentation results. Distance information is combined with probability model to make the algorithm more flexible for segmentation. Data is varied across the subjects to make the model robust. Global affine and non-rigid registration method is used to register multi-spectral histograms gathered from patients' data with a reference histogram. Experiments are performed on patient's datasets with varying the size, location, shape and texture of the tumor.

Ruan *et al.* [16] proposed a supervised machine learning technique to track the tumor volume. Four different modalities (T1, T2, PD, and FLAIR) are used for segmentation. The complete process is categorized into two main steps. In first step to make it efficient and reducing

computational time, only T1 modality is used to identify the abnormal area. In second step the abnormal area is extracted from all modalities and fused to segment the tumor. SVM is used in both steps to segment the complete tumor.

Corso *et al.* [17] used multimodal brain dataset of 20 expert annotated glioblastoma multiforme (GBM) gathered from different sources. Pre-processing is performed on all the four modalities T1, T1C, T2 and FLAIR. A top down model based approach is used to distribute the product over generative model, where classification and segmentation is performed. In the second step input sparse graph is given to graph cut method, where each edge uses features to find similarity between neighbouring nodes having the affinity. Segmentation by weighted aggregation (SWA) is used in graph cut method to provide the multi-level segmentation of data, where each voxel is classified into one of the three (active tumor, necrotic or edema) classes and at higher level these voxel are combined as single segment.

Fluid vector flow (FVF) [12] is the technique introduced to address the problem of unsatisfactory capture range and poor convergence for concavities. FVF showed improvement over gradient vector flow (GVF), boundary vector flow (BVF) and ACM on different datasets to get concave shapes and capture great range. The dataset used for experimentation is either collected from online repository or synthetic images.

Harati *et al.* [9] demonstrated an improved fuzzy connectedness (FC) algorithm, where seed points are selected automatically to segment the tumor region. The algorithm does not depend on tumor type in terms of pixel intensity. To define an object in an image, the strength of connectedness between every pair of image element is calculated, which is determined by considering all possible connected paths among the pair. Results are evaluated based on

similarity index (SI), overlap fraction and extracted fraction. The method is useful to automatically predict the size and position of brain tumor.

Sachdeva *et al*. [11] used texture information with intensity in ACM to overcome the issue observed in previous techniques like FVF, BVF and GVF. In previous techniques selection of false edges or false seeds correspond to pre-convergence problem and selection of weak edges lead to over-segmentation due to the edema around the tumor. Texture space for brain tumor segmentation is defined in gray level matrix.

Zhu *et al.* [13] proposed a semi-automatic brain tumor segmentation method, in which initial segmentation is performed through ITK-Snap tool. Voxel based segmentation and deformable shape based segmentation are combined into the software pipeline. Voxel based is used as an automatic segmentation and deformable shape based segmentation manually refine it. GBM patients' dataset with T1C and T2 modality only is used and results are further refined by using post-processing step.

Automatic segmentation is performed using the random forest (RF) [15], where features extraction is performed after pre-processing and before each voxel classification. Features include MR sequence intensities, neighbourhood information, context information and texture. Post-processing is performed for the sake of good results.

ACM combine the edge based and region based techniques [18], where user draws ROI in different images on the basis of tumor type and grade. ACM is implemented using level set method, which allows merging and splitting.

Reza and Iftekharuddin used intensity and intensity difference features with novel texture features in [19]. Texture based features include fractal piece-wise triangular prism surface area

(PTPSA) and multi-fractional brownian motion (mBm) and then after the fusion of all extracted features, classical RF is applied to segment brain into different regions.

No.	Authors	Modalities	Method	Accuracy	Time	S
1	Rexilius *et al*, 2007	T1C, T2, FLAIR	Region growing + Multi-spectral histogram model adaption	0.73 (Jaccard)	10m	SA
2	Ruan *et al*, 2007	T1, T2, FLAIR, PD	Multi-modality MRI with SVM Classification	0.99 (True Positive)	5m	FA
3	Corso *et al*, 2008	T1, T1C, T2, FLAIR	Generative affinity model and graph cut method are used with SWA	0.62 - 0.69 (Jaccard)	7m	FA
4	Wang *et al*, 2009	T1	FVF and brain tumor segmentation	0.6 (Tanimoto)	5s	SA
5	Harati *et al*, 2011	T1C	Fully automatic Fuzzy Connectedness algorithm	0.93 (Similarity Index)	2.5 m	FA
6	Sachdeva *et al*, 2012	T1, T1C, T2	Texture features + ACM	72% - 98%	-	SA
7	Zhu *et al*, (2012)	T1C, T2	Software pipeline with post-processing	0.25 – 0.81 (Jaccard)	4 m	SA
8	Silva *et al*, 2013	MICCAI BRATS 2013	Multi-sequence MRI using RF	0.83 (Dice)	20 – 25 m	FA
9	Zhao *et al*, 2013	MICCAI BRATS 2013	MRF + Supervoxels	0.83 (Dice)	4 m	FA
10	Binsheng *et al*, 2013	MICCAI BRATS 2013	Semi-automatic segmentation using ACM	0.54 - 0.94 (Dice)	1 m	SA

Table 1: Brain tumor segmentation by machine learning or edge/region based algorithm. Different dataset is used except in last three rows. FA denotes fully automatic and SA denotes semi-automatic [1].

Method	Description	Supervision	Year
Bauer	Hierarchical RF classification and Conditional Random Field (CRF) regularization	FA	2012
Geremia	Spatial RF for semantic image classification	FA	2012
Humamci	Cellular Automaton (CA) based segmentation + Graph theoretic methods	SA	2012
Menze (D)	Generative Discriminative Model (GDM) building on top of Menze (G)	FA	2012
Shin	Hybrid clustering and classification by logistic regression	FA	2012
Subbanna	Hierarchical MRF approach with Gabor features	FA	2012
Zhao (I)	Learned MRF on Supervoxels clusters	FA	2012
Zikic	Context-sensitive features with a decision tree ensemble	FA	2012
Cordier	Patch-based tissue segmentation approach	FA	2013
Doyle	Hidden Markov Model (HMM) and variational Energy Minimization (EM) in a generative model	FA	2013
Festa	RF classifier over local context and neighbourhood features	FA	2013
Guo	ACM with user involvement	FA	2013
Meier	Voxel based feature extraction with spatial regularization	FA	2013
Reza	Fractal PTPSA and mBm with RF	FA	2013
Tustison	Concatenation of RF model with open source Advanced Normalization Tools (ANTs)	FA	2013
Zhao (II)	MRF over Supervoxels	FA	2013

Table 2: Algorithms using FA or SA methods and presented in 2012 and 2013 BraTS challenge.

It is still a challenging task to automatically segment tumor from brain. Saha *et al.* [20] proposed a fast novel method to locate the bounding box around tumor or edema using Bhattacharya [21] coefficient. In their proposed clustering technique axial view of brain image is divided into left and right halves, then a rectangle is used to compare the corresponding regions of left half with right half to find the most dissimilar region within the rectangle and similar outside the rectangle. Irfan *et al.* [22] introduced a technique in which brain images are separated from non-brain part, then ROI is used with the saliency information to bound the search of Normalization cut (N-Cut) [23] method. Saliency information is the combination of multi-scale contrast and image curvature points, in multi-scale image is decomposed at multiple levels with Gaussian Pyramid (GP) and window size of 5*5 is used at various scales to calculated the Euclidean distance with neighbouring pixels, which results multi-contrast image.

In machine learning availability of benchmark data became important in comparing a specific task among different algorithms. Recently this idea has also become famous in the domain of medical image analysis. Sometime challenge word is used instead of benchmark that shares the common characteristic in a sense that different researchers used their own algorithms and optimize that on a training dataset provided by the organizers of event and then apply their algorithm to a common, independent test dataset. The benchmark idea is different from other published comparisons in a sense that in benchmark each group of researchers uses the same dataset for their algorithm, while in others each group of researchers uses the dataset and size of data of their own choice, so difficult to compare.

The BraTS benchmark was established in 2012 and first event was held in the same year. Dataset consists of real and simulated images, where real images are the patients' images and simulated images are made from website i.e. Brainweb. Initially in 2012 it was binary class problem

(edema and core), Later in 2013, it was enhanced to multi-class (background, necrosis, edema, enhancing and non-enhancing). Online evaluation tool is available to test individuals' algorithm while label of test data are kept private. Evaluation process will always remain same after the benchmark established. Table 2 categorize the algorithms on the basis of FA/SA and the year in which algorithm presented in competition.

Various studies presented different accuracy in their papers as shown in Table 1, but it is difficult to draw conclusion about the best technique. Researcher used either FA or SA technique with different dataset and pre-processing/post-processing steps, therefore it is not straightforward to compare them. In previous study value of Dice and Jaccard was not very high and there is room for further improvement in classification accuracy, therefore we explored wavelet based texture features which were not explored before on this dataset.

Chapter 3 : Proposed Methodology

3 Proposed Methodology

In this chapter we describe the proposed fully automatic algorithm, which uses MICCAI BraTS dataset and apply pre-processing steps on data before feature extraction. Random decision forest is applied on extracted features to perform classification. The main flow of our proposed technique is given in Figure 4.

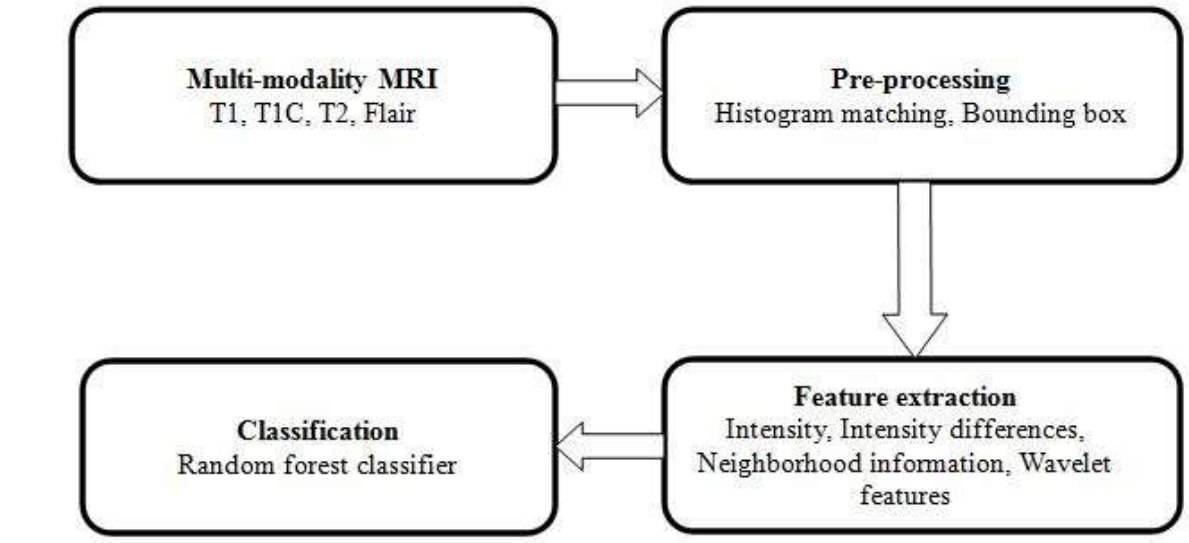

Figure 4: Block diagram of proposed methodology.

3.1 Pre-processing

The used dataset has four modalities of MRI; T1, T2, T1C and FLAIR. Every other modality within a subject is rigidly co-registered with T1C modality to homogenize data, because T1C has the highest spatial resolution in most cases. Linear interpolator is used to resample all the images to 1 mm isotropic resolution in axial orientation. Images are skull-stripped with expert annotation

as shown in Figure 5 [14]. All images are visualized through ITK-Snap [24] and then histogram matching is performed with Slicer3D [25] by taking the best contrast image as reference.

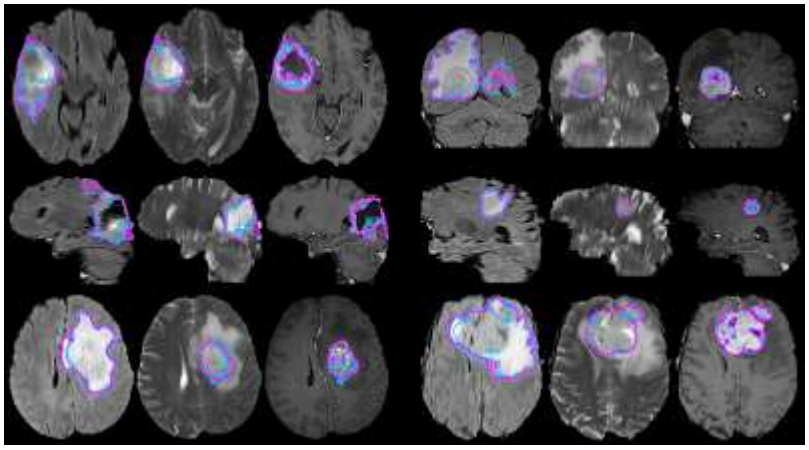

Figure 5: BraTS training data example with expert annotation. Data of three modalities is shown, where left two columns denote whole tumor on FLAIR, center two columns denote core tumor in T2 and right two columns shows active tumor in T1C.

Our adapted technique for locating bounding box consists on following four steps as shown in Figure **6**.

i. Remove complete blank (intensity value 0) slices from ground truth, remaining slices contain tumor part as in Figure 6a
ii. Create a mask as shown in Figure 6b
iii. Use mask to crop ground truth in rectangle (most zeros will be removed here) as in Figure 6c
iv. Apply mask to crop multimodality images of that subject as shown in Figure 6e

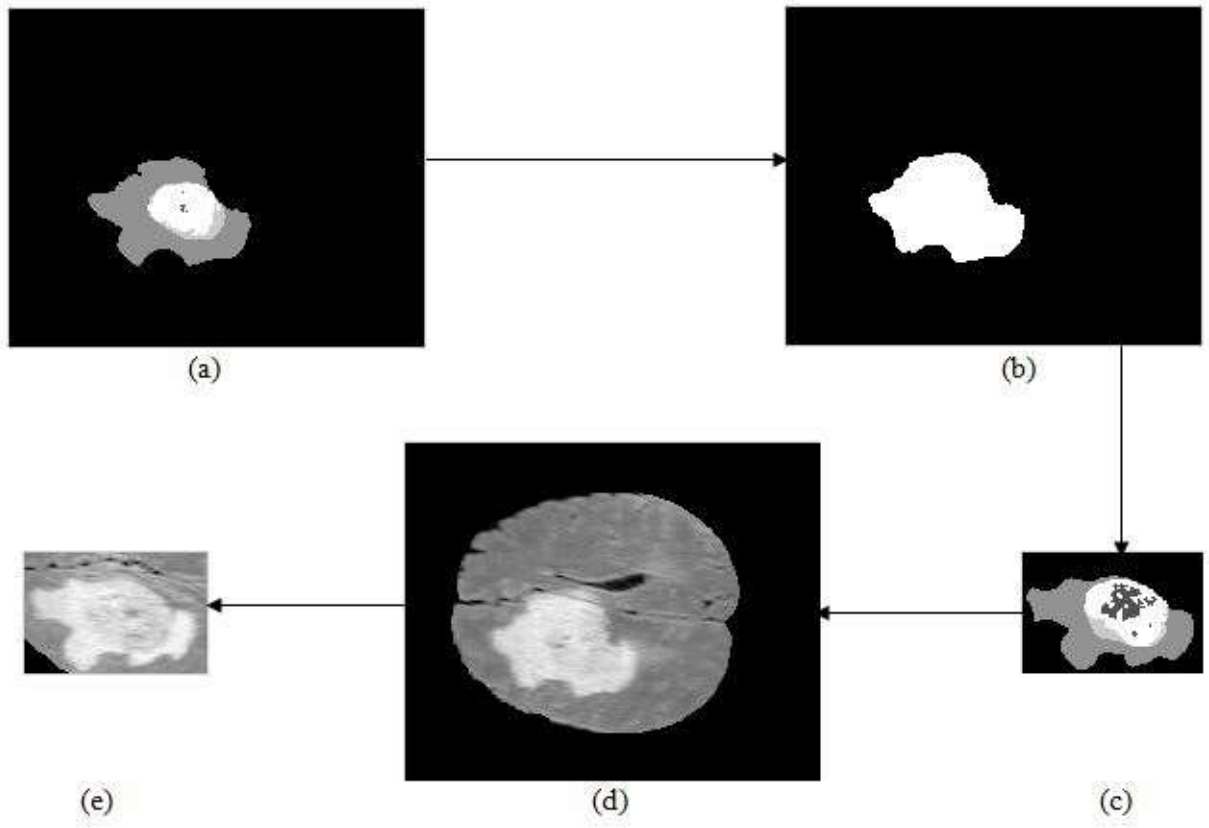

Figure 6: Bounding box method of proposed methodology: (a) Ground truth image, (b) Mask of ground truth, (c) Bounding box of ground truth, (d) A slice of FLAIR, (e) Cropped slice of FLAIR after applying bounding box.

3.2 Feature Extraction

The proposed feature extraction includes four types of features: (i) intensity, (ii) intensity difference, (iii) neighbourhood information and (iv) wavelet based texture features. Each modality of a subject is a 3D volume having voxel intensity values. Each 3D volume is reshaped to 1D to represent a feature vector as in [15] and [19]. Each subject has four modalities and there will be 1D feature vector for each modality, therefore total four modalities combine and make four features as shown in Figure **7**.

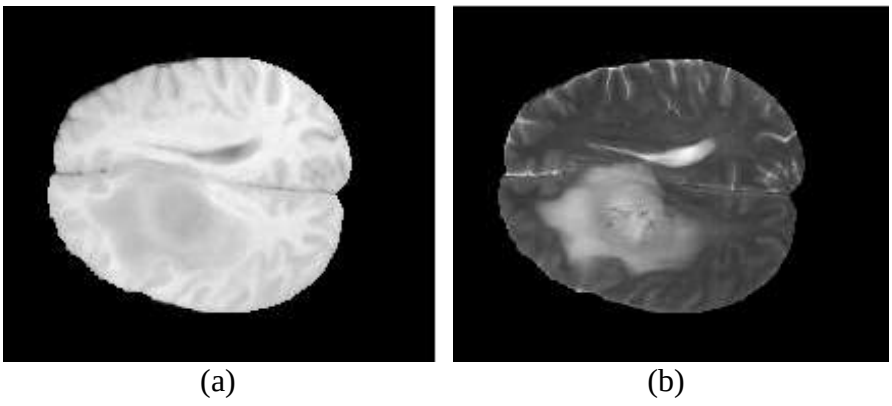

(a) (b)

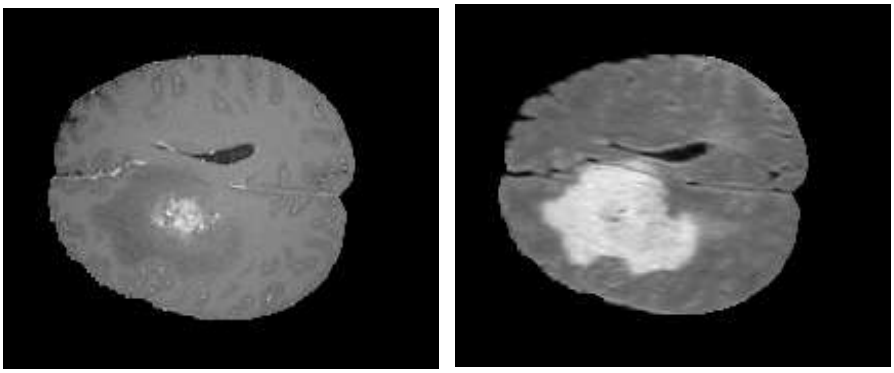

(c) (d)

Figure 7: Multi-modality scans of a subject: (a) T1, (b) T2, (c) T1C, (d) FLAIR

Intensity difference are all the differences between the above four modalities, also used by [15] and [19]. There are six forward and six backward differences (e.g. FLAIR-T1 and T1-FLAIR), which yield twelve features. We initially used all of them and draw a feature importance graph shown in Figure 8 to know the most important intensity difference features.

Figure 8 shows the importance of all the intensity and intensity difference features, which are extracted and ranked on the basis of importance of each feature in model creation. In our approach we used only 3 intensity difference features that are highly ranked as shown in Figure 9. Our feature vector dimensions increased to 7 by adding 3 intensity difference features.

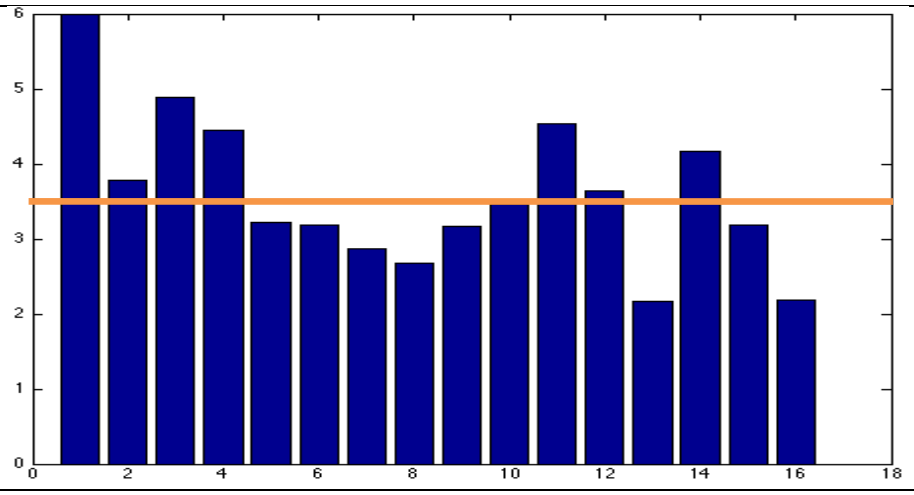

Figure 8: First four (from left) are intensity features and the remaining twelves are intensity difference features. We used only highly ranked (the normalized standard deviation score of the difference between ooBError before and after permutation over all trees) intensity difference features.

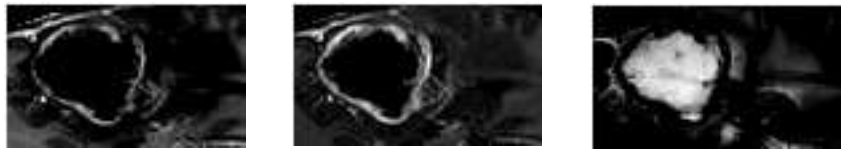

Figure 9: Intensity differences: (a) T1C-FLAIR, (b) T1C-T1, (c) T2-T1C

Neighbourhood information features include mean, median and range of 3D neighbours centred at voxel being considered. We vary the length of edges to 3, 9, 15 and 19 mm for mean and range, while median filter uses only edges of length 3. We analysed that the above mentioned number of edges are best for our classification. Total 36 neighbourhood information features are calculated for mean, median and range filter on multimodality images. The previous 7 features of intensity and intensity difference are combined with 36 neighbourhood information features to make FV of size 43 for each voxel [15].

The novelty of the proposed approach is to extract wavelet features, which has not been explored and applied on MICCAI BraTS dataset. Wavelet is used in data compression, signal processing, numerical analysis and image denoising without major degradation. It has the property of multi-

resolution analysis, where we can decompose and visualize the images at different scales [26]. Time and frequency information are used to visualize transient image structure. Discrete wavelet transform can be defined in equation $\mathbf{W_{j,k}(t) = 2^{\frac{-j}{2}}\vartheta_0(2^{-j}t - k)}$---------- , where $j, k \in Z$, j controls dilation and k controls translation.

Wavelet decomposition is achieved by performing scaling and shifting on initial wavelet and convolving it with the original image. It has the property to reconstruct the original image without loss of information [27]. Multi-resolution analysis is the significant property of wavelet transform, which provides the detail information of image at various scales. The scaling function is used in decomposition and reconstruction process for down-sampling (removing samples) and up-sampling (adding interpolated samples) [28]. The scaling and wavelet functions are given as,

$$\boldsymbol{\varphi_{j,k}(t) = 2^{\frac{-j}{2}}\varphi_0(2^{-j}t - k)}\text{---------- (1)}$$

$$\mathbf{W_{j,k}(t) = 2^{\frac{-j}{2}}\vartheta_0(2^{-j}t - k)}\text{---------- (2)}$$

where $\varphi_{j,k}(t)$ is a scaling function and $W_{j,k}(t)$ is a wavelet function, j is used to control dilation and k controls translation.

Block diagram of wavelet based feature extraction is shown in Figure 10. In wavelet based feature extraction, an image (from T1C, T1C-FLAIR, T1C-T1 or T2-T1C) is given as input for 3D wavelet decomposition. Input image is decomposed into subbands and only those subbands containing useful information are then selected based on visual analysis. Feature images are reconstructed from selected subband and then Gaussian filter is applied after absolute function to make the edges of feature images more prominent.

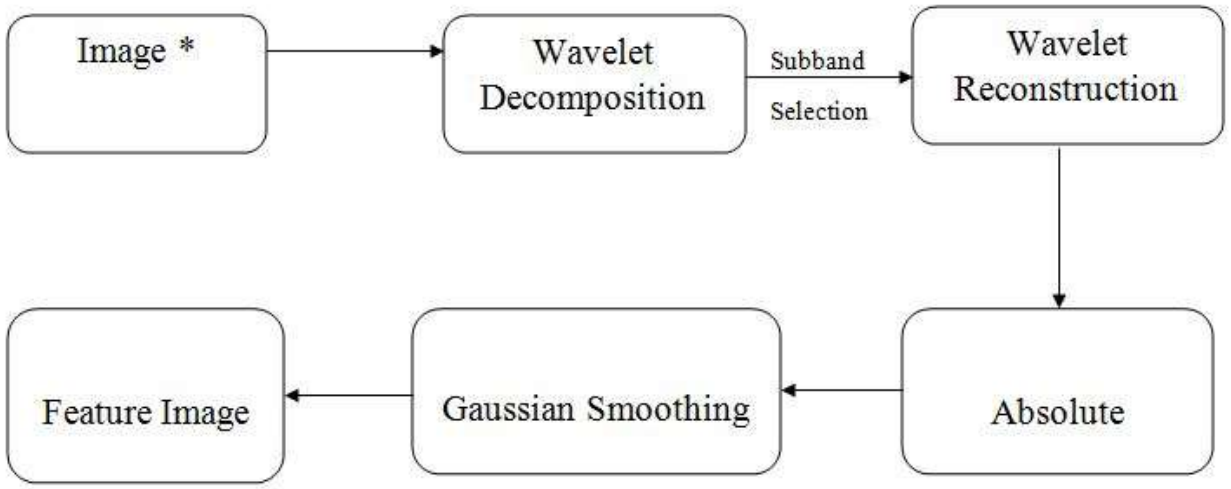

Figure 10: Block diagram of wavelet based feature extraction, * represent that image can be FLAIR – T1C, T1 – T1C, T1C – T2 or T1C [29].

Figure 11 shows 3D wavelet decomposition at level 1. Level 2 is achieved by further decomposing the LLL subband having detail information. L is for low frequency and H is for high frequency, so in 3D volume LLL is the subband having low frequency contents from all dimensions and LLH having low frequency in x and y directions and high frequency in z direction. In 1D, the signal is filtered in x dimension only, while in 2D, the image is filtered in x dimension first to produce low pass and high pass sub-images, where low pass is filtered again in y dimension to produce LL, LH, HL and HH. In 3D, the volume is initially filtered in x dimension which results in sub-volumes as low pass and high pass, both sub-volumes are filtered in y dimension which produce four sub-volumes, which are again filtered in z dimension to produce 8 sub-volumes LLL, LLH, LHL, HLL, LHH, HLH, HHL, HHH [27].

Initially we performed decomposition at 3rd level, but after visualizing subbands we decided to restrict at 2nd level, because subbands of 3rd level were not useful for us. We tried various filter families for wavelet decomposition including daubechies4, symlets4 and symlets8, while we used symlets8 for our wavelet decomposition, because it was providing best contrast.

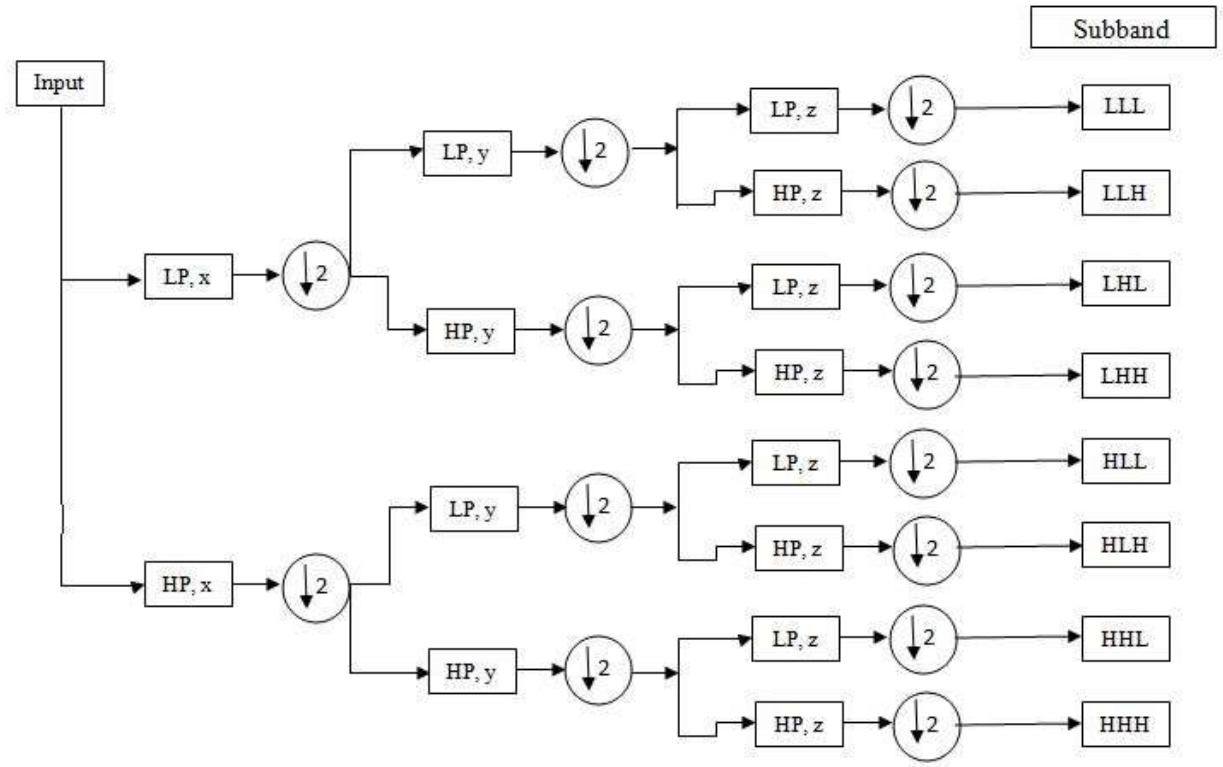

Figure 11: Block diagram of 3D wavelet decomposition at level 1, where LP denotes low pass filter and HP denotes high pass filter respectively [30]. L is for low frequency and H is for high frequency.

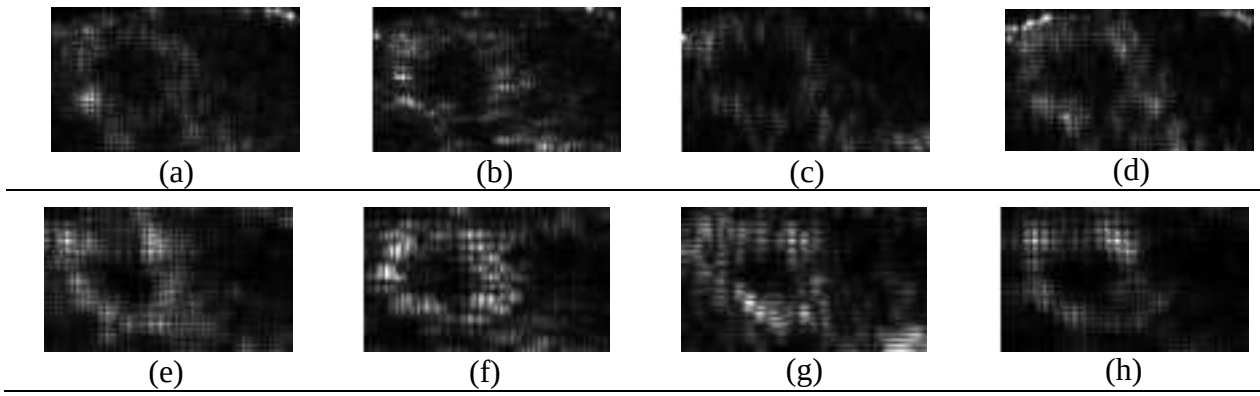

Figure 12: Selected feature images where H denotes high frequency and L denotes low frequency respectively: (a) HHH1, (b) HHL1, (c) HLH1, (d) LHH1, (e) HHH2, (f) HHL2, (g) HLH2, (h) LHH2.

Wavelet reconstruction is a process in which feature image are constructed from each subband. Feature images are selected based on the visual analysis and discriminatory information. We

applied absolute function and Gaussian smoothing to make the edges of feature images more prominent [29] as shown in Figure 12.

Only 8 subbands are selected for each of the 4 input images (from T1C, FLAIR-T1C, T1-T1C or T1C-T2) to make FV of size 32. Wavelet based extracted features are added into the previously calculated, which increased the dimensionality of FV to 75. We extracted intensity, intensity differences, neighbourhood information and wavelet based texture features. In the next section we will use these extracted features to perform supervised classification.

3.3 Classification

Supervised classification is a machine learning approach in which training data is used to construct the model and test data is used to test the constructed model on unknown data to evaluate the performance of algorithm. There are a number of classifiers that exist to classify data, but we will discuss those classifiers below which we have explored for our dataset. These include kNN, random forest, AdaBoost, and random under sampling boost (RusBoost) classifiers.

The **kNN** classifier is a supervised learning technique, which takes training data as input to create model. It keeps all the training data in training phase and in test phase it calculates Euclidean distance of test sample with each training sample to select those samples which exist in define range. The kNN is a lazy learning technique, it is much fast in training phase and slow in testing phase, therefore it is ignored in many applications i.e. dynamic web mining [31]. Predicted output is calculated by majority class among nearest-neighbours,

$$\mathbf{Distance}(\mathbf{x},\mathbf{y}) = \sqrt{\sum_{\mathbf{i=1}}^{\mathbf{n}}(\mathbf{x_i} - \mathbf{y_i})^{\mathbf{2}}} \text{---------- (3)}$$

Euclidean distance between test sample and all the training samples is calculated to select the closest k-neighbors.

Random forest (RF) is a combination of decision trees. Each tree in ensemble is trained on randomly sampled data with replacement from training vector during the phase of training. Bootstrap aggregation technique is used during the training phase of RF. In bootstrap aggregation, multiple trees are trained on a training data to increase the correlation and reduce the variance between trees, because training on single tree is sensitive to noise and causes over-fitting. The parameters should be kept in mind while growing trees, very deep trees are highly varied so they overfit training and generate irregular patterns. RF reduces the variance by the concept of training different parts of same dataset and averaging these trees [32]. RF provides us information about the important of each extracted feature after model creation. In test phase unknown data is provided to individual trees for classification. RF considers votes of all the trees and gives the majority vote as classification [33].

$$\mathbf{Result} = {}^{\mathbf{1}}\!/_{\mathbf{B}} \times \sum_{\mathbf{b=1}}^{\mathbf{B}} \mathbf{T_b}\ (\mathbf{x}') \text{---------- (4)}$$

Where 'B' is the number of trees, T_b is the decision tree and x' is the test sample. Test sample is given to each decision tree through iteration and label according to a majority vote is given to the test sample.

AdaBoostM2 is the enhanced version of AdaBoostM1 and used for multiclass classification. It is the boosting algorithm, where many weak learners are combined to make a powerful algorithm and instances are reweighted rather than resampled (in bagging). In the training phase weight is assigned to each sample and decision tree is grown on the basis of weight owned by these samples.

$$\mathbf{F_N(x)} = \sum_{\mathbf{n=1}}^{\mathbf{N}} \mathbf{f_t(x)} \text{ ---------- (5)}$$

AdaBoostM2 is the combination of many weak learners as f_t in the above equation, x is the sample used by weak learners and returns the target class. AdaBoostM2 uses pseudo-loss instead

of learning rate for all observations, which increases at slow rate after few iterations and approaches to 0.5 [34].

Random under sampling (RusBoost) is best for classifying imbalanced data when instances of one class dominate many times than the other. Machine learning techniques fail to efficiently classify skew data, but RusBoost solved the problem by combining sampling and boosting. It counts the number of observations of each class and takes ratio of every other class with reference to the smallest class for training. Training samples are initialized with the weight which is updated by iterating through all weak learners and learning rate [35]. Ensemble creation and learning rate is same as in AdaBoostM2.

$$\mathbf{H(x)} = \underset{\mathbf{y} \in \mathbf{Y}}{\mathbf{argmax}} \sum_{\mathbf{n=1}}^{\mathbf{N}} \mathbf{h_t(x, y)} \times \mathbf{log}\frac{\mathbf{1}}{\boldsymbol{\alpha}_\mathbf{n}} \text{ ---------- (6)}$$

We used BraTS dataset and visualized multi-modality MRI through ITK-snap to select the one with best histogram. We performed histogram matching for all other subjects by keeping the subject with best histogram as a reference subject using Slicer3D. Then we take bounding box of ground truth and applied that on all modalities to remove extra part from images. RF is applied on four types of extracted features (intensity, intensity differences, neighbourhood and wavelet based texture) to evaluate our algorithm.

Chapter 4 : Results

4 Results

In this chapter we will present our results and compare them with previous work which uses the same dataset. Three measures are used for quantitative evaluation and visual results of segmentation are also shown.

4.1 Out of Bag Error (ooBError)

OoBError is the mean squared error or the misclassification error for our of bag observations in training. There is no need of separate test set of cross-validation to get the unbiased estimated error for test cases, because ooBError is calculated internally during RF model creation phase. Each tree in RF is created from independently drawn bootstrap replica of input data. Observations not included in this replica are called ooBError for this tree also known as the probability of misclassification [36]. Figure 13 show that ooBError is lowest when 25 trees are used.

4.2 Hierarchical Classification

Each voxel is classified as one of the target class and then hierarchical regions are computed from those class labels. We computed three regions as follows:

Whole Tumor: This region is the combination of four classes (1+2+3+4), which are separated from class 0.

Tumor Core: In this region we separate combination of three (1+3+4) classes from edema (2).

Enhancing Tumor: It has only one class 4 which is separated from the combination of two classes (1+3).

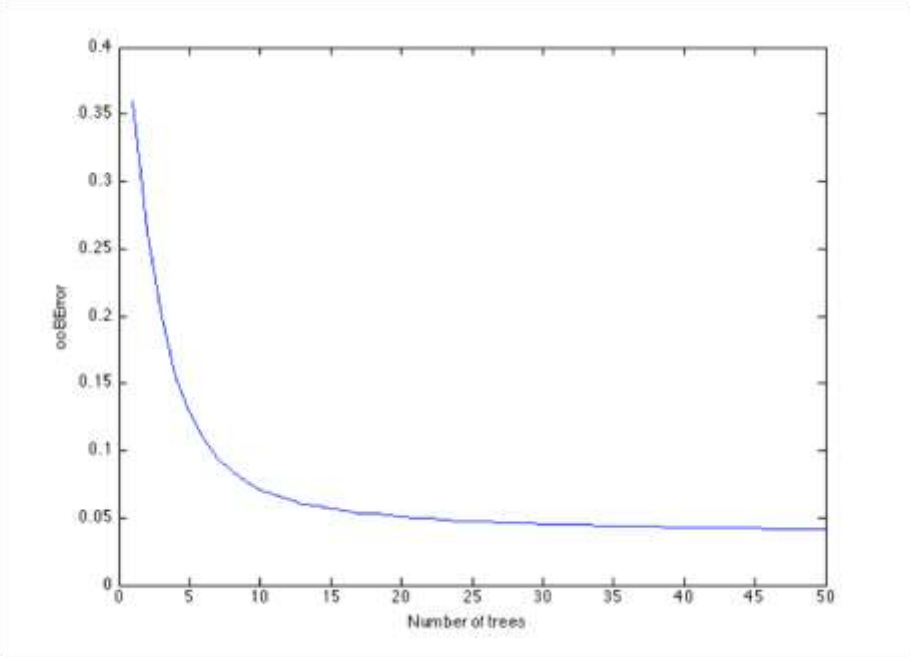

Figure 13: Graph is showing relationship between number of trees and ooBError. OoBError decreasing rapidly till the number of trees equal to 25 and then it's becoming steady.

Region	Intensity	Intensity + Intensity Diff.	Intensity + Intensity Diff + Neighbourhood	Intensity + Intensity Diff + Neighbourhood + Wavelets
Complete	0.80	0.81	0.83	0.85
Core	0.90	0.90	0.92	0.93
Active	0.85	0.90	0.91	0.91
Complete	0.90	0.90	0.91	0.91
Core	0.61	0.62	0.66	0.67
Active	0.97	0.97	0.99	0.99
Complete	0.89	0.89	0.90	0.90
Core	0.77	0.75	0.78	0.80
Active	0.96	0.96	0.94	0.94
Complete	0.92	0.92	0.92	0.92
Core	0.70	0.70	0.73	0.76
Active	0.87	0.88	0.89	0.90

Table 3: Segmentation is performed on each type of features to analyse the importance of extracted features. Results are calculated on 4 real HG patients.

Wavelet based texture feature has improved our results and to justify this we performed cross-validation on 4 real HG patients and the Dice score is calculated on the basis of each type of feature set. Wavelet based texture features are compared with other features as shown in Table 3. Ensemble classifier often outperforms an individual classifier [37]. We compared KNN, RF, RusBoost and AdaBoostM2 and analysed that RF gave best results among all as shown in Table 4, where Dice percentage is calculated by performing leave-one-out cross validation on four real patient's data.

Region	Random Forest	KNN	AdaBoost M2	RusBoost
Complete	0.85	0.85	0.84	0.87
Core	0.93	0.92	0.46	0.92
Active	0.91	0.92	1.00	0.91
Complete	0.91	0.90	0.91	0.91
Core	0.67	0.48	0.64	0.67
Active	0.99	0.93	1.00	0.98
Complete	0.90	0.88	0.90	0.89
Core	0.80	0.69	0.80	0.74
Active	0.94	0.65	0.97	0.94
Complete	0.92	0.93	0.92	0.92
Core	0.76	0.43	0.40	0.64
Active	0.90	0.75	0.84	0.88

Table 4: Comparison of RF, KNN, AdaBoostM2 and RusBoost (Leave-one-out cross validation). Results are shown for 4 HG real patients.

4.3 Evaluation Measures

We have calculated Dice similarity coefficient to compare our results with other researchers' work. Dice coefficient is the similarity/overlap between two images [38]. It is graphically explained in Figure 14 and mathematically,

$$\mathbf{Dice}(\mathbf{P},\mathbf{T}) = \frac{(\mathbf{2} * |\mathbf{P_1} \cap \mathbf{T_1}|)}{(|\mathbf{P_1}| + |\mathbf{T_1}|)} \text{ ---------- (7)}$$

In above equation ′ ∩ ′ is the logical AND operator, | | is the size of the set (i.e., the number of voxels belonging to it). P1 and T1 represent the number of voxels belong to algorithm's predicted and ground truth respectively. The Dice score normalizes the number of true positives to the average size of predicted and ground truth segmented area. It also gives us the voxel wise overlap between the result and ground truth [14].

Jaccard coefficient measures the similarity between two images and can be defined as the size of intersection divided by the size of union of two sets [39]. Jaccard coefficient is also known as Jaccard index and can be measured as,

$$\mathbf{Jaccard}(\mathbf{P},\mathbf{T}) = \frac{|\mathbf{P_1} \cap \mathbf{T_1}|}{|\mathbf{P_1} \cup \mathbf{T_1}|} \text{ ---------- (8)}$$

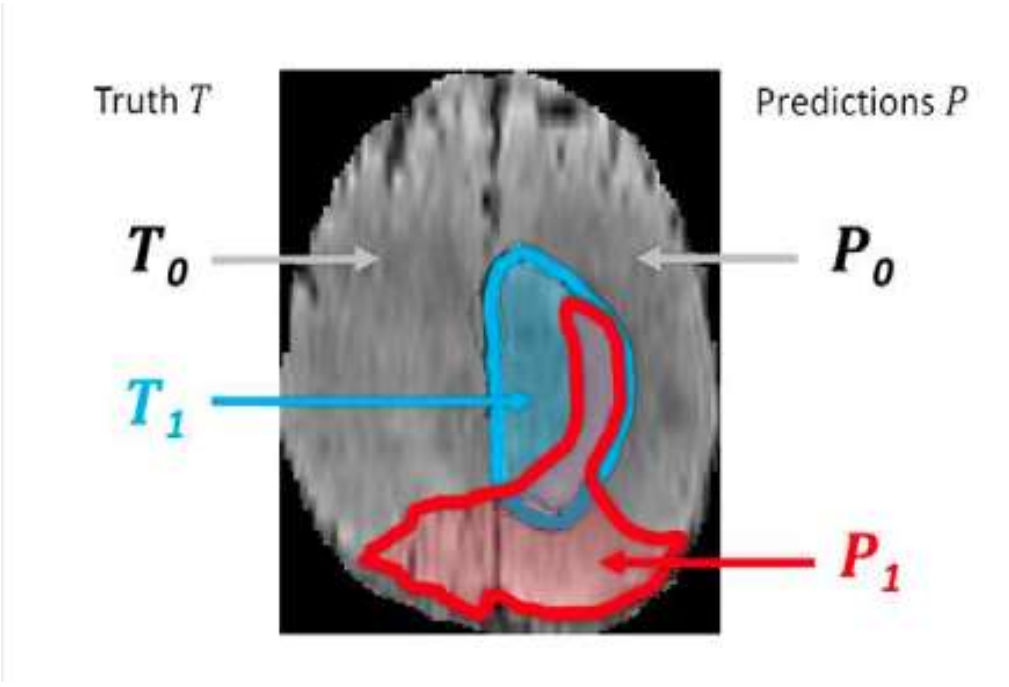

Figure 14: Dice score is calculated by deriving formula from the diagram. Blue is the true lesion labeled as T1, T0 is the area outside T1 but not black. P1 is the red color area predicted by algorithm and P0 is the non-black area outside P1. Overlapped area between T1 and P1 gives us the number true positive [14].

Sensitivity is true positive rate [14], it is prioritized when disease is serious and we want to identify all the possible true cases. It can be measured as,

$$\mathbf{Sensitivity}(\mathbf{P},\mathbf{T}) = \frac{|\mathbf{P_1} \cap \mathbf{T_1}|}{|\mathbf{T_1}|} \text{ ---------- (9)}$$

Specificity is true negative rate [14], it is prioritized when treatment is dreadful and we only want to treat those, which are surely having disease. It can be measured,

$$\mathbf{Specificity}(\mathbf{P},\mathbf{T}) = \frac{|\mathbf{P0} \cap \mathbf{T0}|}{|\mathbf{T0}|} \text{ ---------- (10)}$$

4.4 Quantitative Evaluation

The quantitative results of BraTS challenge held in 2012 and 2013 are shown on real dataset in Table 5 and Table 6 respectively. Results of proposed methodology are compared with other in Table 7 and Table 8 is used for the detailed results of proposed technique, which are obtained on hp-probook 4540s, core i5, 2.5 GHz, 8 GB RAM using MATLAB 2013a and it takes about 2 minutes to test a new patient.

Real data, Dice in %	Whole Tumor	Core Tumor
Bauer	60	29
Geremia	61	23
Hamamci	69	37
Shin	32	9
Subbanna	14	25
Zhao (I)	34	37
Zikic	70	25

Table 5: Dice similarity coefficient results of MICCAI BraTS 2012 on real data [14].

Real data, Dice in %	Whole Tumor	Core Tumor	Active Tumor
Cordier	84	68	65
Doyle	71	46	52
Festa	72	66	67
Meier	82	73	69
Reza	83	72	72
Tustison	87	78	74
Zhao (II)	84	70	65

Table 6: Dice similarity coefficient results of MICCAI BraTS 2013 on real data [14].

S. No.	Author	Whole (HG)	Core (HG)	Active (HG)	Whole (LG)	Core (LG)	Time (minutes)
1	Bauer	74	54	57	49	30	8 (CPU)
2	Doyle	78	45	42	63	41	15 (CPU)
3	Festa	77	56	61	24	33	30 (CPU)
4	Guo	75	67	49	71	59	<1 (CPU)
5	Menze	76	59	54	**81**	58	20 (CPU)
6	Reza	77	50	55	52	39	90 (CPU)
7	Subbanna	82	**75**	59	55	54	70 (CPU)
8	Tustison	78	60	52	68	42	100 (Cluster)
9	Zhao	84	68	49	78	60	15 (CPU)
10	**Proposed Methodology**	**88**	**75**	**95**	**81**	**62**	<2 (CPU)

Table 7: Comparison of our results with other researcher's work on BraTS dataset [14].

Similarity Measure	Whole (HG)	Core (HG)	Active (HG)	Whole (LG)	Core (LG)
Dice	0.88	0.75	0.95	0.81	0.62
Jaccard	0.79	0.65	0.91	0.69	0.48
Specificity	0.86	0.81	0.89	0.83	0.55
Sensitivity	0.95	0.90	0.94	0.87	0.72

Table 8: Detailed results of proposed method by measuring different metrics on HG and LG data.

4.5 Visual Results

Segmentation results of other researchers are shown in Figure 15 and Figure 16 and segmentation results of the proposed method are shown in **Error! Reference source not found.**.

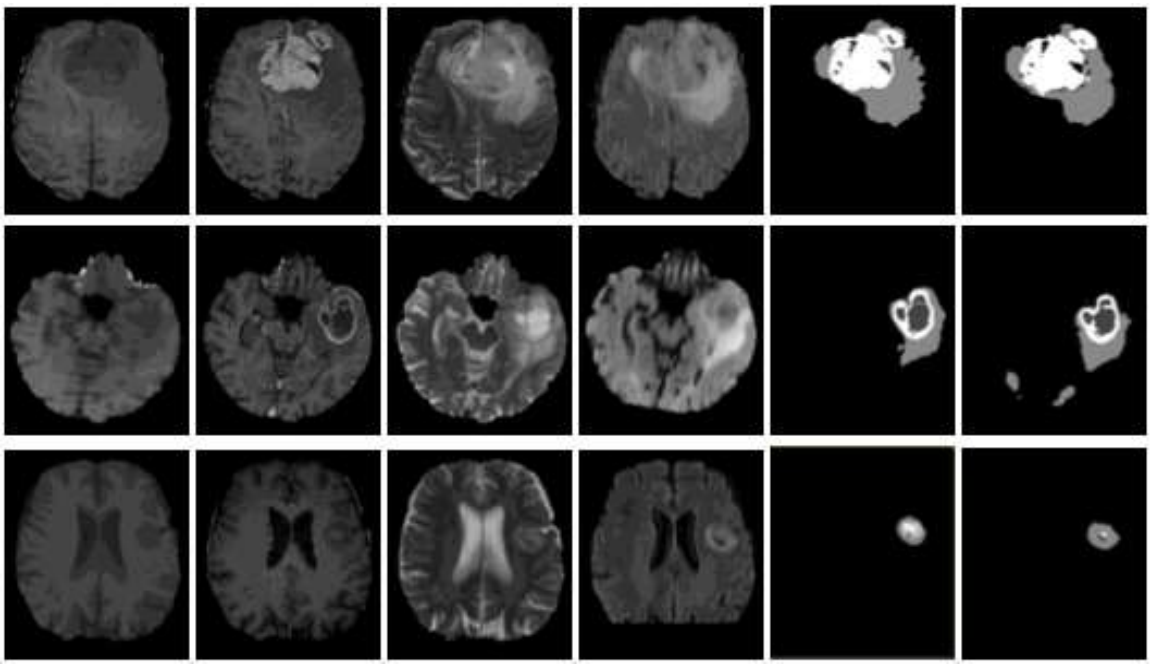

Figure 15: Tumor segmentation example of three different subjects [15]. From left to right (a) T1, (b) T1C, (c) T2, (d) FLAIR, (e) Ground Truth, (f) Festa's [15] predicted results.

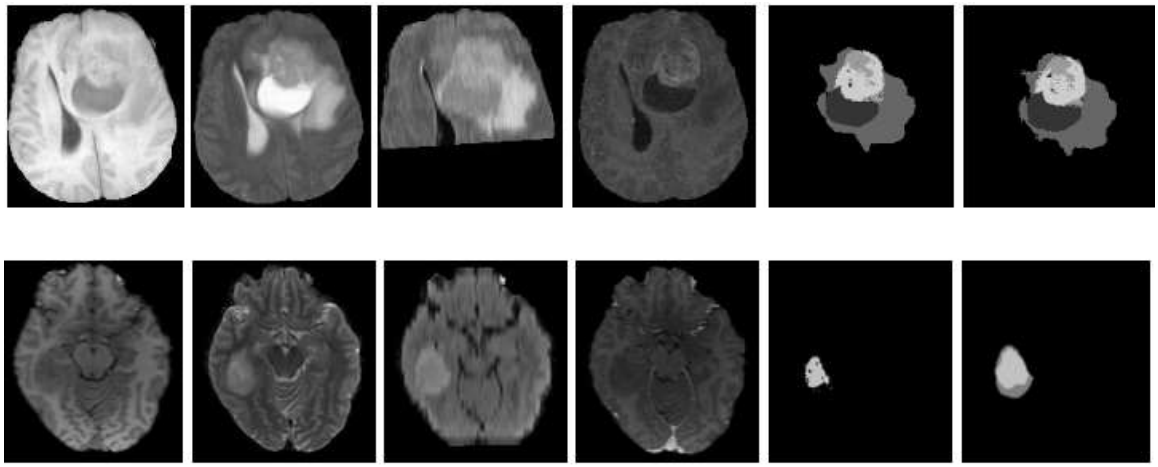

Figure 16: Segmentation results of two patients; (a) T1, (b) T2, (c) FLAIR, (d) T1C, (e) Reza's [19] Segmented results, (f) Ground truth.

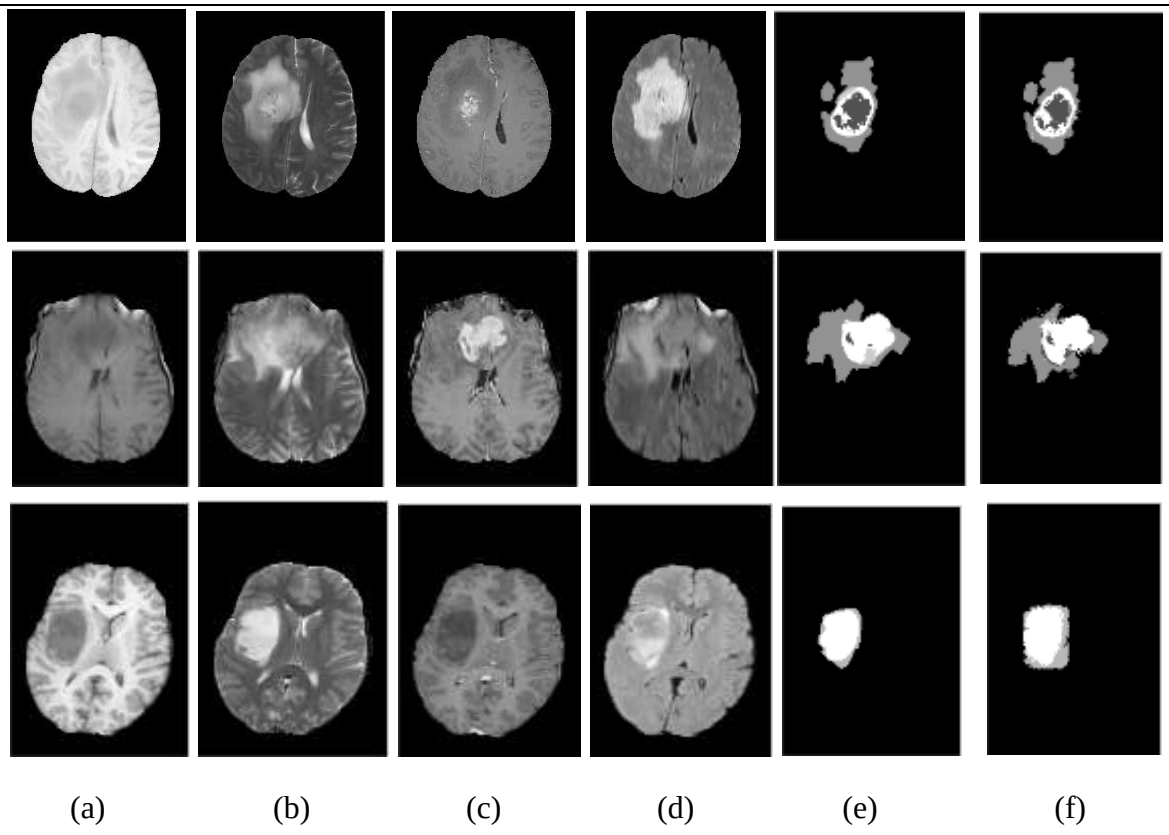

Figure 17**:** Segmentation results of proposed methodology. Each row represents a patient's brain images. (a) T1, (b) T2, (c) T1C, (d) FLAIR, (e) Ground truth and (f) Proposed method's results.

4.6 Discussion

In this thesis, we proposed an automatic way to segment and classify the brain tumor from multi-modality MRI scans. It utilizes multi-modality MRI scans to extract features like intensity, intensity differences and neighbourhood information, which are also explored by Festa *et al.* [15]. Our technical contribution in this research is to add wavelet features, which increase the Dice co-efficient and improves the results.

We compared different classifiers (kNN, RF, AdaBoostM2 and RusBoost) in Table 4 and come to know that RF is best for our extracted features to segment and classify brain tumor. Detailed classification of tumor is more difficult than the segmentation of complete tumor, so we performed detailed classification and classify the tumor into three different regions (complete tumor, core tumor and enhancing tumor.

Conclusion and Future Work

Conclusion and Future Work

Fully automatic machine learning algorithm has been proposed in this work to hierarchically classify the tumor into three regions. Intensity, intensity difference, neighborhood information and wavelet features are extracted and utilized with machine learning classifier. The use of wavelet based texture features has enhanced the Dice coefficient and the results of our proposed methodology are comparable to the state of the art.

Beside accuracy and time complexity, future work can test the algorithm on larger dataset to verify robustness of this algorithm. Furthermore, automatic subband selection from wavelet subbands for feature extraction can be explored.

Appendices

Appendix

I Brain Tumor

Brain tumor is the growth of abnormal tissues in the brain. Normally in human body old cells are damaged and new cell are created to take their place. When new cells are formed without the need and old cells are not damaged then the extra cells form a mass of tissues called a tumor as in Figure 18. Brain tumor can be benign or malignant, benign tumor is easy to cure as compared to malignant because it is less severe, having clear tumor boundary and do not spread into the other part of body [40].

II Tumor Grades

Tumor cell is divided into four grades by clinicians according how the cell appears under the microscope [1]. World Health Organization (WHO) introduced grading scheme on the basis of tumor severity. Grade I cells look normal as compared to Grade II cells. Tumor starts growing actively in Grade III and called GBM (most severe tumor stage) in Grade IV. Higher the grade of tumor has lesser the chance of survival. Grade I and II are categorized as low grade while grade III and IV are high grade [40]. Low grade becomes high grade with the passage of time and in high grade patient is near to death [41]. Image of low grade and high grade is shown in Figure 19.

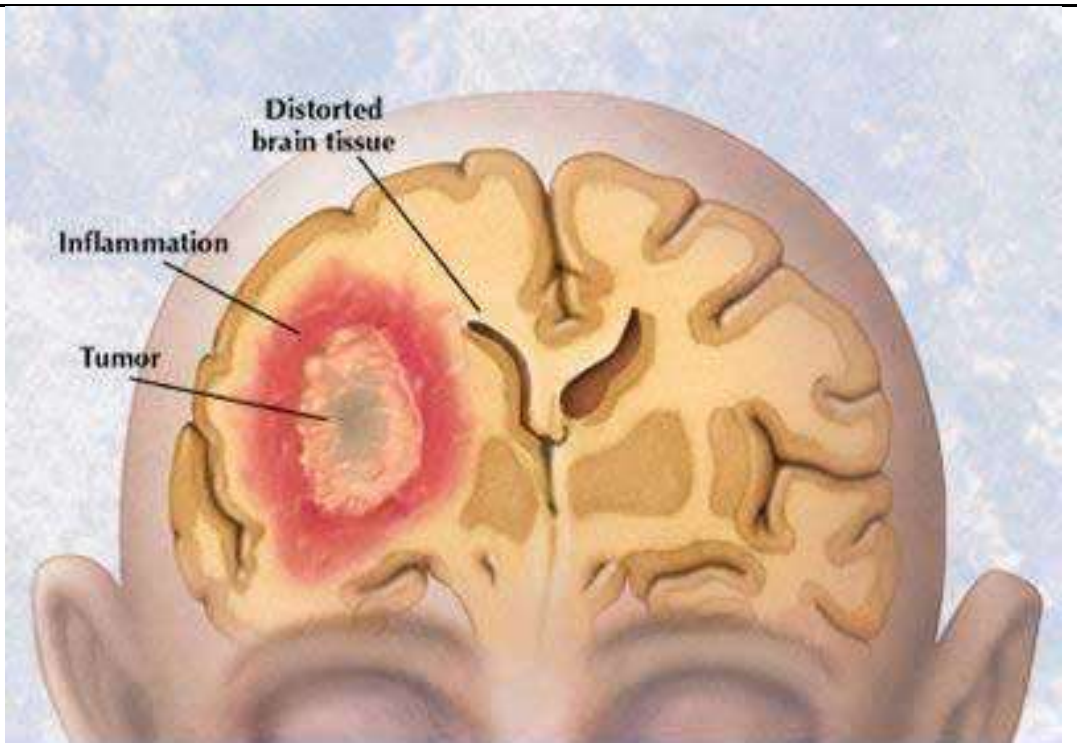

Figure 18: Image of human brain where tumor is in centre of red circle [42].

III Symptoms of Brain Tumor

Blood circulates continuously to and from brain. In case the tumor blocks the blood then signs of brain tumor e.g. headache, vomiting, problem in walking and memory loss may occur.

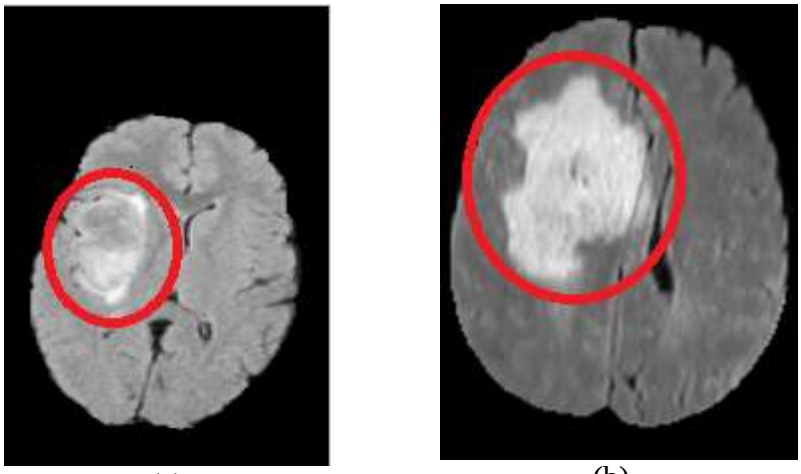

(a) (b)

Figure 19: MRI images of a patient taken from MICCAI BraTS dataset; (a) Low grade tumor, (b) High grade tumor.

References

[1] S. Bauer, R. Wiest, L.-P. Nolte, and M. Reyes, "A survey of MRI-based medical image analysis for brain tumor studies," *Physics in medicine and biology,* vol. 58, p. R97, 2013.

[2] B. A. Kohler, E. Ward, B. J. McCarthy, M. J. Schymura, L. A. Ries, C. Eheman, A. Jemal, R. N. Anderson, U. A. Ajani, and B. K. Edwards, "Annual report to the nation on the status of cancer, 1975–2007, featuring tumors of the brain and other nervous system," *Journal of the National Cancer Institute,* 2011.

[3] R. Siegel, D. Naishadham, and A. Jemal, "Cancer statistics, 2013," *CA: a cancer journal for clinicians,* vol. 63, pp. 11-30, 2013.

[4] A. S. o. C. Oncology. (2005, May 8). *Types of Cancer*. Available: http://www.cancer.net/cancer-types/brain-tumor

[5] ct-scan-info.com. (2007, 13 May). *MRI vs CT Scan*. Available: http://www.ct-scan-info.com/mrivsctscan.html

[6] J. H. Medicine. (2005, May 8). *Health Library*. Available: http://www.hopkinsmedicine.org/healthlibrary/conditions/adult/nervous_system_disorders/brain_tumors_85,P00775/

[7] G. G. College. (2011, May 8). *Neuroscience and Physiological Psychology*. Available: http://wiki.ggc.edu/wiki/Neuroscience_and_Physiological_Psychology

[8] Philips. (2015, May 9). *Health Care*. Available: http://www.healthcare.philips.com/main/products/mri/systems/achieva3t/

[9] V. Harati, R. Khayati, and A. Farzan, "Fully automated tumor segmentation based on improved fuzzy connectedness algorithm in brain MR images," *Computers in biology and medicine,* vol. 41, pp. 483-492, 2011.

[10] J. Rexilius, H. K. Hahn, J. Klein, M. G. Lentschig, and H.-O. Peitgen, "Multispectral brain tumor segmentation based on histogram model adaptation," in *Medical Imaging*, 2007, pp. 65140V-65140V-10.

[11] J. Sachdeva, V. Kumar, I. Gupta, N. Khandelwal, and C. K. Ahuja, "A novel content-based active contour model for brain tumor segmentation," *Magnetic resonance imaging,* vol. 30, pp. 694-715, 2012.

[12] T. Wang, I. Cheng, and A. Basu, "Fluid vector flow and applications in brain tumor segmentation," *Biomedical Engineering, IEEE Transactions on,* vol. 56, pp. 781-789, 2009.

[13] Y. Zhu, G. S. Young, Z. Xue, R. Y. Huang, H. You, K. Setayesh, H. Hatabu, F. Cao, and S. T. Wong, "Semi-automatic segmentation software for quantitative clinical brain glioblastoma evaluation," *Academic radiology,* vol. 19, pp. 977-985, 2012.

[14] B. Menze, M. Reyes, and K. Van Leemput, "The Multimodal Brain TumorImage Segmentation Benchmark (BRATS)," 2014.

[15] J. Festa, S. Pereira, J. A. Mariz, N. Sousa, and C. A. Silva, "Automatic Brain Tumor Segmentation of Multi-sequence MR images using Random Decision Forests," *Proceedings MICCAIBRATS,* 2013.

[16] S. Ruan, S. Lebonvallet, A. Merabet, and J. Constans, "Tumor segmentation from a multispectral MRI images by using support vector machine classification," in *Biomedical Imaging: From Nano to Macro, 2007. ISBI 2007. 4th IEEE International Symposium on*, 2007, pp. 1236-1239.

[17] J. J. Corso, E. Sharon, S. Dube, S. El-Saden, U. Sinha, and A. Yuille, "Efficient multilevel brain tumor segmentation with integrated bayesian model classification," *Medical Imaging, IEEE Transactions on,* vol. 27, pp. 629-640, 2008.

[18] X. Guo, L. Schwartz, and B. Zhao, "Semi-automatic Segmentation of Multimodal Brain Tumor Using Active Contours," *Multimodal Brain Tumor Segmentation,* p. 27, 2013.

[19] S. Reza and K. Iftekharuddin, "Multi-class Abnormal Brain Tissue Segmentation Using Texture," *Multimodal Brain Tumor Segmentation,* p. 38, 2013.

[20] B. N. Saha, N. Ray, R. Greiner, A. Murtha, and H. Zhang, "Quick detection of brain tumors and edemas: A bounding box method using symmetry," *Computerized medical imaging and graphics,* vol. 36, pp. 95-107, 2012.

[21] D. Comaniciu, V. Ramesh, and P. Meer, "Real-time tracking of non-rigid objects using mean shift," in *Computer Vision and Pattern Recognition, 2000. Proceedings. IEEE Conference on*, 2000, pp. 142-149.

[22] I. Mehmood, N. Ejaz, M. Sajjad, and S. W. Baik, "Prioritization of brain MRI volumes using medical image perception model and tumor region segmentation," *Computers in biology and medicine,* vol. 43, pp. 1471-1483, 2013.

[23] J. Shi and J. Malik, "Normalized cuts and image segmentation," *Pattern Analysis and Machine Intelligence, IEEE Transactions on,* vol. 22, pp. 888-905, 2000.

[24] P. A. Yushkevich, J. Piven, H. C. Hazlett, R. G. Smith, S. Ho, J. C. Gee, and G. Gerig, "User-guided 3D active contour segmentation of anatomical structures: significantly improved efficiency and reliability," *Neuroimage,* vol. 31, pp. 1116-1128, 2006.

[25] R. Kikinis and S. Pieper, "3D Slicer as a tool for interactive brain tumor segmentation," in *Engineering in Medicine and Biology Society, EMBC, 2011 Annual International Conference of the IEEE*, 2011, pp. 6982-6984.

[26] M. Sifuzzaman, M. Islam, and M. Ali, "Application of wavelet transform and its advantages compared to Fourier transform," 2009.

[27] A. Procházka, L. Gráfová, O. Vyšata, and N. Caregroup, "Three-Dimensional Wavelet Transform in Multi-Dimensional Biomedical Volume Processing," in *Proc. of the IASTED Int. Conf. Graphics and Virtual Reality, Cambridge, UK*, 2011.

[28] R. Polikar, "The wavelet tutorial," 1996.

[29] K. M. Rajpoot and N. M. Rajpoot, "Wavelets and support vector machines for texture classification," in *Multitopic Conference, 2004. Proceedings of INMIC 2004. 8th International*, 2004, pp. 328-333.

[30] S. Cai, K. Li, and I. Selesnick, "Matlab implementation of wavelet transforms," *Retrieved March,* vol. 28, p. 2009, 2002.

[31] G. Guo, H. Wang, D. Bell, Y. Bi, and K. Greer, "KNN model-based approach in classification," in *On The Move to Meaningful Internet Systems 2003: CoopIS, DOA, and ODBASE*, ed: Springer, 2003, pp. 986-996.

[32] J. Friedman, T. Hastie, and R. Tibshirani, *The elements of statistical learning* vol. 1: Springer series in statistics Springer, Berlin, 2001.

[33] L. Breiman, "Random Forests," *Machine Learning,* vol. 45, pp. 5-32, 2001/10/01 2001.

[34] Y. Freund and R. E. Schapire, "A decision-theoretic generalization of on-line learning and an application to boosting," *Journal of computer and system sciences,* vol. 55, pp. 119-139, 1997.

[35] C. Seiffert, T. M. Khoshgoftaar, J. Van Hulse, and A. Napolitano, "RUSBoost: improving classification performance when training data is skewed," in *Pattern Recognition, 2008. ICPR 2008. 19th International Conference on*, 2008, pp. 1-4.

[36] M. W. Mitchell, "Bias of the Random Forest out-of-bag (OOB) error for certain input parameters," *Open Journal of Statistics,* vol. 1, p. 205, 2011.

[37] M. Shaheryar, M. Khalid, and A. M. Qamar, "Rot-SiLA: A Novel Ensemble Classification approach based on Rotation Forest and Similarity Learning using Nearest Neighbor Algorithm," in *Machine Learning and Applications (ICMLA), 2013 12th International Conference on*, 2013, pp. 46-51.

[38] L. R. Dice, "Measures of the amount of ecologic association between species," *Ecology,* vol. 26, pp. 297-302, 1945.

[39] P. Jaccard, "The distribution of the flora in the alpine zone," *New phytologist,* vol. 11, pp. 37-50, 1912.

[40] N. C. Institute. (2012, May 9). *Brain Tumor*. Available: http://www.cancer.gov/global/web/policies

[41] P. Kleihues, P. C. Burger, and B. W. Scheithauer, "The new WHO classification of brain tumours," *Brain pathology,* vol. 3, pp. 255-268, 1993.

[42] C. P. Devis. (2013, May 8). *Health Cure*. Available: http://healthcuresimplified.blogspot.com/2013/06/brain-tumor.html